THE MINERALOGICAL DISTRIBUTION OF GOLD AND RELATIVE TIMING OF GOLD MINERALIZATION IN TWO ARCHEAN SETTINGS OF HIGH METAMORPHIC GRADE IN AUSTRALIA

PETER NEUMAYR

Key Centre for Strategic Mineral Deposits, Department of Geology, The University of Western Australia,
Nedlands, W.A. 6009, Australia

LOUIS J. CABRI

Mineral Sciences Laboratories, CANMET, 555 Booth Street, Ottawa, Ontario K1A 0G1

DAVID I. GROVES AND EDWARD J. MIKUCKI

Key Centre for Strategic Mineral Deposits, Department of Geology, The University of Western Australia,
Nedlands, W.A. 6009, Australia

JENNIFER A. JACKMAN

Metals Technology Laboratories, CANMET, 568 Booth Street, Ottawa, Ontario K1A 0G1

ABSTRACT

Gold in Archean lode-gold deposits at Mt. York (Pilbara Craton) and Griffin's Find (Yilgarn Craton), in Western Australia, located in amphibolite- and lower granulite-facies domains, respectively, is associated with composite arsenopyrite – löllingite grains. In combination, reflected-light microscopy, scanning electron microscopy (SEM), and secondary-ion mass spectrometry (SIMS) reveal the mineralogical distribution of gold and the timing of gold mineralization relative to the peak of metamorphism. In both deposits, composite arsenopyrite – löllingite grains are distinctly zoned, with arsenopyrite generally rimming a core of löllingite. Native gold, where present, is preferentially located at grain boundaries between arsenopyrite and löllingite. SIMS analysis demonstrates that the majority of the gold occurs as "invisible" gold in löllingite, whereas arsenopyrite is essentially free of such gold. Textural relationships confirm that gold was precipitated together with löllingite, broadly synchronously with the peak of metamorphism in both lode-gold deposits. The gold was concentrated preferentially at the arsenopyrite – löllingite grain boundaries during replacement of löllingite by arsenopyrite, under slightly retrograde metamorphic conditions, apparently due to the inability of the arsenopyrite structure to accommodate the gold at these still relatively high temperatures. This study demonstrates that gold was initially coprecipitated with löllingite under high P–T conditions and that the particulate (visible) gold, alone, does not indicate the true paragenetic position of initial deposition of gold in these deposits.

Keywords: refractory gold, invisible gold, secondary-ion mass spectrometry, löllingite, arsenopyrite, amphibolite–granulite-facies gold deposits, Mt. York, Griffin's Find, Western Australia.

SOMMAIRE

L'or des gisements aurifères archéens de Mt. York (socle de Pilbara) et de Griffin's Find (socle de Yilgarn), en Australie occidentale, situés dans des domaines recristallisés aux facies amphibolite et granulite inférieur, respectivement, sont associés avec des agrégats zonés d'arsénopyrite et de löllingite. Les résultats combinés obtenus par microscopie en lumière réfléchie, microscopie électronique à balayage, et spectrométrie de masse des ions secondaires (SIMS) documentent la distribution de l'or et situent l'événement minéralisateur dans le temps par rapport à la culmination métamorphique. Dans les deux cas, l'arsénopyrite forme une couronne autour d'un coeur de löllingite. L'or natif est situé surtout à l'interface entre arsénopyrite et löllingite. Les analyses par SIMS montrent que la plus grande partie de l'or se trouve sous forme "invisible" dans la löllingite, tandis que l'arsénopyrite n'en contiendrait peu ou pas. Les relations texturales confirment que l'or a été déposé en même temps que la löllingite, et à peu près en même temps que la culmination métamorphique aux deux endroits. L'or a été concentré de préférence aux interfaces entre arsénopyrite et löllingite lors du remplacement de cette dernière par l'arsénopyrite, sous conditions de métamorphisme légèrement rétrograde. Ce phénomène serait dû à l'incapacité de la structure de l'arsénopyrite à accommoder l'or à ces températures relativement élevées. Notre étude montre que l'or aurait d'abord coprécipité avec la löllingite sous conditions de température et pression élevées, et que la distribution de l'or en particules (or visible), considéré en isolation, n'indique pas la position paragénétique correcte de la déposition initiale de l'or dans ces gisements.

(Traduit par la Rédaction)

Mots-clés: or réfractaire, or invisible, spectrométrie de masse par ions secondaires, löllingite, arsénopyrite, gisements d'or, facies amphibolite–granulite, Mt. York, Griifin's Find, Australie occidentale.

INTRODUCTION

The timing of gold mineralization with respect to the age of its host rocks and of subsequent metamorphic events has been a contentious issue for some time. Although modern consensus now focusses on epigenetic origins for most lode-gold systems, the timing of ore formation relative to metamorphic history still remains problematical in many deposits, especially for deposits hosted in amphibolite- and granulite-facies host rocks. Three different age-relationships have been suggested for high-metamorphic-grade deposits: i) premetamorphic mineralization: *i.e.*, gold mineralization formed at lower temperatures and subsequently metamorphosed (*e.g.*, Kuhn *et al.* 1986, Hamilton & Hodgson 1986, Phillips & de Nooy 1988, Phillips 1990); ii) synmetamorphic mineralization: *i.e.*, gold formed synchronously with the peak of regional metamorphism (*e.g.*, Andrews *et al.* 1986, Burk *et al.* 1986, Colvine *et al.* 1988, Couture & Guha 1990, Barnicoat *et al.* 1991), and iii) postmetamorphic mineralization: *i.e.*, gold formed after the peak of regional metamorphism (*e.g.*, Marmont 1986, Tabeart 1987, 1988, Pan & Fleet 1992). Detailed textural and paragenetic studies are required to unequivocally determine which model, if any, predominates for amphibolite- and granulite-facies gold deposits in general.

Gold in lode-gold deposits occurs either as native gold, commonly within quartz veins (*e.g.*, Robert & Kelly 1987, Boiron *et al.* 1991), or enclosed in hydrothermal silicates, or spatially associated with sulfides (*e.g.*, Wood *et al.* 1986), commonly in altered wallrock next to the veins, as both grains of native gold and refractory (sulfide-hosted, "invisible") gold. Considerable effort has been expended to examine the location, mechanisms of precipitation and timing of native gold in quartz veins, which is shown in several cases to be located in fractures related to late-stage brittle deformation of early quartz (White 1943, Boiron *et al.* 1991). Similarly, the paragenetic relationships of hydrothermal alteration to the associated sulfide mineralization are usually well understood. However, the paragenesis and crystal chemistry of gold-bearing sulfides and sulfarsenides, and the timing of precipitation of native gold relative to the various sulfides and sulfarsenides, are relatively poorly documented. This is partly due to problems with the determination of low concentrations of gold and other trace elements in sulfides. However, advances in analytical techniques, especially the use of secondary-ion mass spectrometry (SIMS) and accelerator mass spectrometry, allow the detection, analysis for gold and mapping of its distribution and that of other trace elements down to a detection limit of a few μg/g in the sulfides (*e.g.*, Chryssoulis *et al.* 1987, 1989, Reed 1989, Wilson *et al.* 1991). These techniques allow, for the first time, unequivocal determination of the paragenetic relationships of gold with respect to those of

associated sulfides and sulfarsenides, and finally places important restrictions on the timing of gold in the hydrothermal system.

In this paper, we examine gold mineralization in two Archean lode-gold deposits, one in the amphibolite facies, and the other in the lower granulite facies, in order to determine the siting and timing of gold relative to the precipitation of ore-related sulfides and peak metamorphic conditions. The location of gold within arsenopyrite – löllingite – pyrrhotite assemblages is examined through reflected light microscopy, scanning electron microscopy (SEM), and secondary ion mass spectrometry (SIMS), and is interpreted in terms of known relationships in the system Fe–As–S. Although petrographic studies on the location of gold within arsenopyrite – löllingite – pyrrhotite assemblages exist in earlier studies (*e.g.*, Lhotka & Nesbitt 1989, Kojonen *et al.* 1991, Kontoniemi *et al.* 1991), this paper is the first one to: i) use EDS and SIMS to gain a believable, quantitative measure of the distribution of both native and invisible gold in the coexisting Fe–As–S phases, and ii) to attempt a detailed explanation of the results.

STUDY AREAS

Mt. York

Gold mineralization in the Mt. York District, eastern Pilbara Craton, Western Australia (Fig. 1), is partly hosted in metamorphosed banded iron-formation (BIF) at the Main Hill – Breccia Hill prospect (Neumayr *et al.* 1994), samples of which have been investigated in this study. Mt. York is located in the Archean Pilgangoora greenstone belt, which largely comprises metamorphosed volcanic rocks of the *ca.* 3.46 Ga (Thorpe *et al.* 1990, McNaughton *et al.* 1993) Warrawoona Group, and metamorphosed, dominantly sedimentary, assemblages of the *ca.* 3.33 Ga (Thorpe *et al.* 1990, McNaughton *et al.* 1993) Gorge Creek Group, including the BIF at the Main Hill – Breccia Hill prospect. The Pilgangoora greenstones have been folded into tight isoclinal folds in a D_{2A} deformation event (Neumayr *et al.* 1994), which was associated with amphibolite-facies metamorphism. A D_{2B} deformation event refolded the greenstone sequences into open, megascopic folds. Gold mineralization at Main Hill – Breccia Hill is spatially associated with NW-plunging F_{2B} buckle folds, and is concentrated along the hanging-wall and footwall contact of the BIF. It is hosted in quartz breccias with a pyrrhotite matrix, associated with composite arsenopyrite – löllingite grains, and with quartz – amphibole veins with bands of arsenopyrite – löllingite paralleling the vein in the adjacent wallrock. Both types of mineralization have been studied; in both types, the alteration is laterally zoned, with distal pyrrhotite (± arsenopyrite) alteration, with pyrrhotite and composite arsenopyrite –
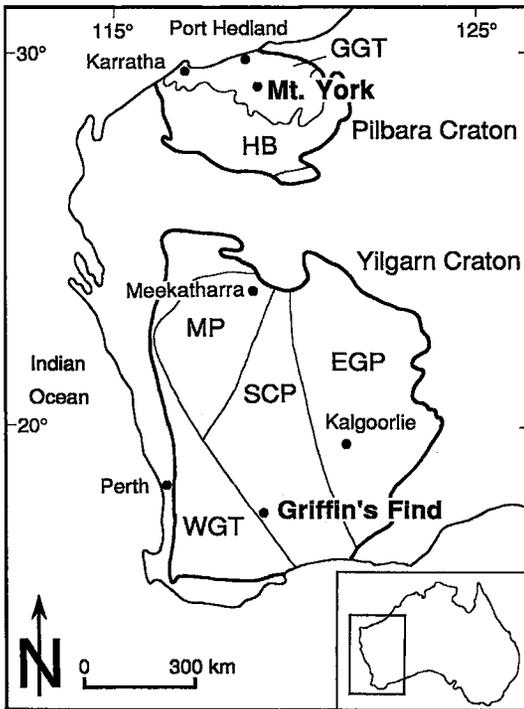
FIG. 1. Map of Western Australia showing the location of Mt. York and Griffin's Find in the Pilbara and Yilgarn Craton (GGT: Granite-Greenstone Terrane; HB: Hamersley Basin; MP: Murchison Province; WGT: Western Gneiss Terrane; SCP: Southern Cross Province; EGP: Eastern Goldfields Province).

löllingite grains increasing in abundance proximal to gold mineralization.

Temperatures derived from biotite – garnet pairs from footwall schists to the BIF indicate 520–640°C for the peak of regional metamorphism (Neumayr et al. 1994). The stabilities of magnesio-hornblende and calcic plagioclase in amphibolites and of grunerite in the BIF also are consistent with amphibolite-facies metamorphism. The stability of andalusite in mica schists in the hanging wall of the BIF limits the pressure to less than 4 kbar (Holdaway 1971).

Griffin's Find

Griffin's Find is located in the Southern Cross Province (Fig. 1), adjacent to the Western Gneiss Terrane of the Yilgarn Craton. The deposit is located in an approximately 3×5 km enclave of greenstone in a granulite-facies granite–gneiss terrane. The hosts to mineralization are interpreted to represent interlayered metamorphosed basalts and sedimentary rocks (Fare 1989). The age of the granulite-facies metamorphism has been determined using conventional U/Pb

zircon analysis as 2634 ± 47 Ma (Wilde & Pidgeon 1987), and the age of gold-related metasomatism, using a Pb/Pb isochron on metamorphic microcline and titanite, as 2635 ± 3 Ma (Fare 1989). Fare (1989) distinguished four events of deformation, with hydrothermal fluids focussed at conditions of peak metamorphism along NW–SE-trending D_4 shears parallel to the fold axis of the kilometer-scale D_1/D_2 folds. Mineralization was deposited at sites of maximum contrast in competency that localized structure-induced permeability and fluid flux. Associated with mineralization are quartz – clinopyroxene veins with quartz – clinopyroxene – manganiferous grossular assemblages in the adjacent wallrock; pyrrhotite, arsenopyrite and löllingite are the main sulfide minerals (Fare 1989, Barnicoat et al. 1991). The mineralization is considered to be syntectonic, as indicated by the presence of both deformed and undeformed quartz – clinopyroxene veins. Garnet – clinopyroxene thermometry of the alteration yields temperatures of about 730–760°C (Fare 1989), whereas temperatures for the peak of metamorphism are estimated as 700–750°C at pressures of 6 ± 1 kbar, utilizing garnet – biotite, garnet – cordierite and garnet – orthopyroxene thermometry (Fare 1989).

METHODOLOGY

Mineralized samples from both the Main Hill – Breccia Hill prospect, Mt. York, and Griffin's Find have been examined with reflected light microscopy to document ore petrology and ore textures (Fig. 2). Selected samples were examined by scanning electron microscopy (SEM) on the JEOL JSM 6400 at the Electron Microscope Centre, University of Western Australia, using secondary electron, as well as backscattered modes, which reveal very small differences in the average atomic number (Z). The acceleration voltage for the imaging was 15 kV, and the beam current 3×10^{-9} nA. The SEM was used to discriminate cryptic compositional zoning in arsenopyrite and löllingite, to detect inclusions of gold and other phases in the Fe–As-sulfides and Fe-arsenides, and to determine exact locations of gold inclusions, where present. Inclusions of gold in composite arsenopyrite – löllingite grains from Mt. York have been analyzed on the SEM, using a LINK EDS X-ray analysis system, a normally incident beam, a take-off angle of 40° and a counting time of 60 seconds. The acceleration voltage for the analysis was 20 kV, and the beam current, 3×10^{-9} nA.

Three samples were selected and subsequently investigated with a Cameca IMS-4f Secondary Ion Mass Spectrometer (SIMS) at the Canada Centre for Mineral and Energy Technology, Ottawa, to determine whether submicroscopic gold is present in arsenopyrite and löllingite. A Cs^+ primary beam (net 14.5 kV) was used for sputtering the carbon-coated samples.
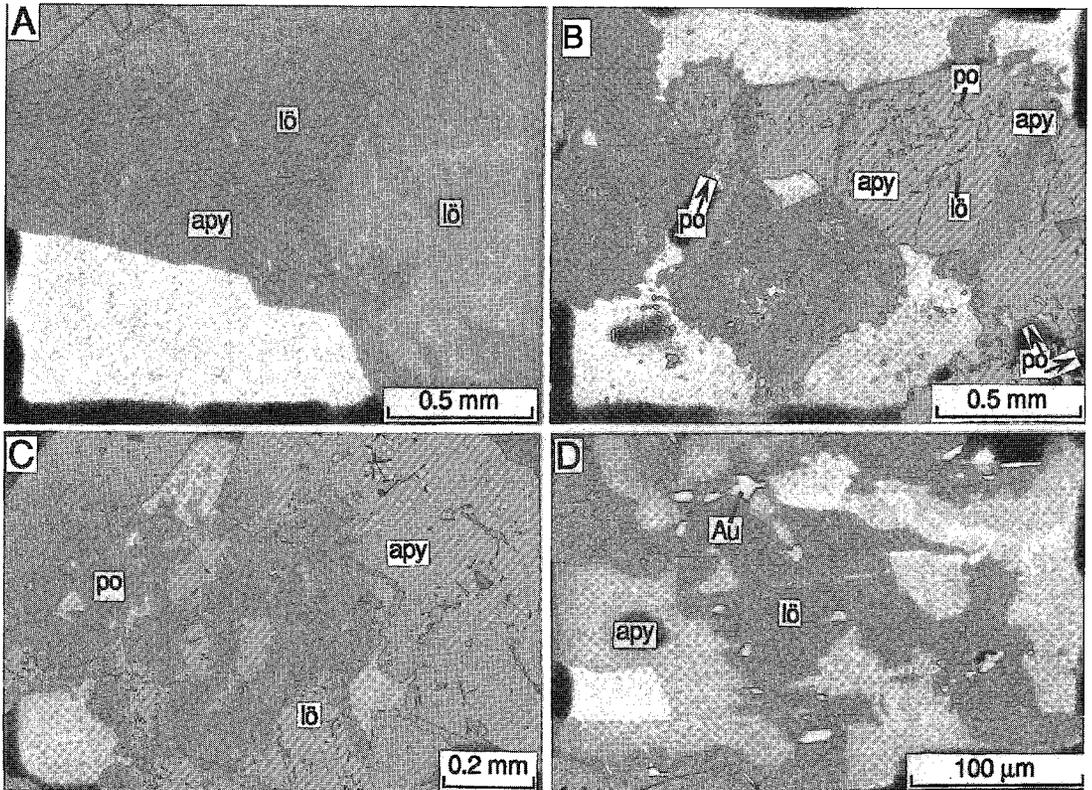
Fig. 2. Photomicrographs and SEM images of sulfide alteration and gold mineralization at Griffin's Find (A) and Mt. York (B, C, D). A. löllingite grains in different optical orientation are rimmed by arsenopyrite in one optical orientation (photomicrograph, reflected light, crossed polars); B. löllingite partially replaced by arsenopyrite, which is itself brecciated and cemented by later arsenopyrite (photomicrograph, reflected light, crossed polars); C. löllingite cores rimmed by arsenopyrite; note grains of native gold at small remnant of löllingite (SEM, back-scattered image); D. löllingite replaced by arsenopyrite with several grains of native gold (bright phase) located at the arsenopyrite – löllingite grain boundary (SEM, back-scattered image). Symbols: apy arsenopyrite, lö löllingite, po pyrrhotite, Au native gold.

Quantitative analyses for gold were obtained by measuring negative secondary ions. Direct images of the distribution of Au, As, and S ions are depicted in Figure 3. Analyses of smaller areas (8 and 25 μm in diameter) in depth-profiling mode (80–100 nA primary beam) within 250-μm rastered square areas were done on individual grains, with results as depicted in Figure 4. The intensity of Au counts in the depth profiles was monitored against different ions (e.g., $^{32}S_2$, $^{56}Fe^{75}As$, and $^{56}Fe_2^{75}As$) and calibrated using external Au-implanted matching mineral standards (Chryssoulis et al. 1989). For each implant standard (dose = 2.5 × 10^{13} atoms/cm^2, implanted at an energy of 1.0 MeV), a Relative Sensitivity Factor (RSF) is obtained. The RSF is defined to be:

$$\text{Au concentration}_{\text{Standard}} \ (\text{atoms/cm}^3)/\text{Au counts}_{\text{Standard}} \times \text{Matrix ion counts}_{\text{Standard}}.$$

Normalization to a matrix species corrects for variations in beam current, etc. The RSF was typically obtained by averaging two or three depth profiles in the standards (Table 1). The Au concentration in the unknown samples was obtained by:

$$\text{Au concentration (atoms/cm}^3) = \text{Au counts}_{\text{Unknown}} \times \text{RSF/Matrix ion counts}_{\text{Unknown}}.$$

Conversion to μg/g in Table 2 (using ρ[löllingite] = 7.2 g/cm^3 and ρ[arsenopyrite] = 6.0 g/cm^3) was obtained as follows:

$$\text{Au concentration}_{\text{Löllingite}} \ (\mu g/g) = \text{Au concentration}_{\text{Löllingite}} \ (\text{at/cm}^3) \times 4.54 \times 10^{-17},$$

and

$$\text{Au concentration}_{\text{Arsenopyrite}} \ (\mu g/g) = \text{Au concentration}_{\text{Arsenopyrite}} \ (\text{at/cm}^3) \times 5.45 \times 10^{-17}.$$

High mass-resolution (M/ΔM between 4,000 and 4,800) was used to detect and avoid the molecular interferences (FeAsS$_2$ and CsS$_2$ ions) that occur very close to the mass of Au (Chryssoulis 1989, Cabri & Chryssoulis 1990). It was not necessary to introduce,
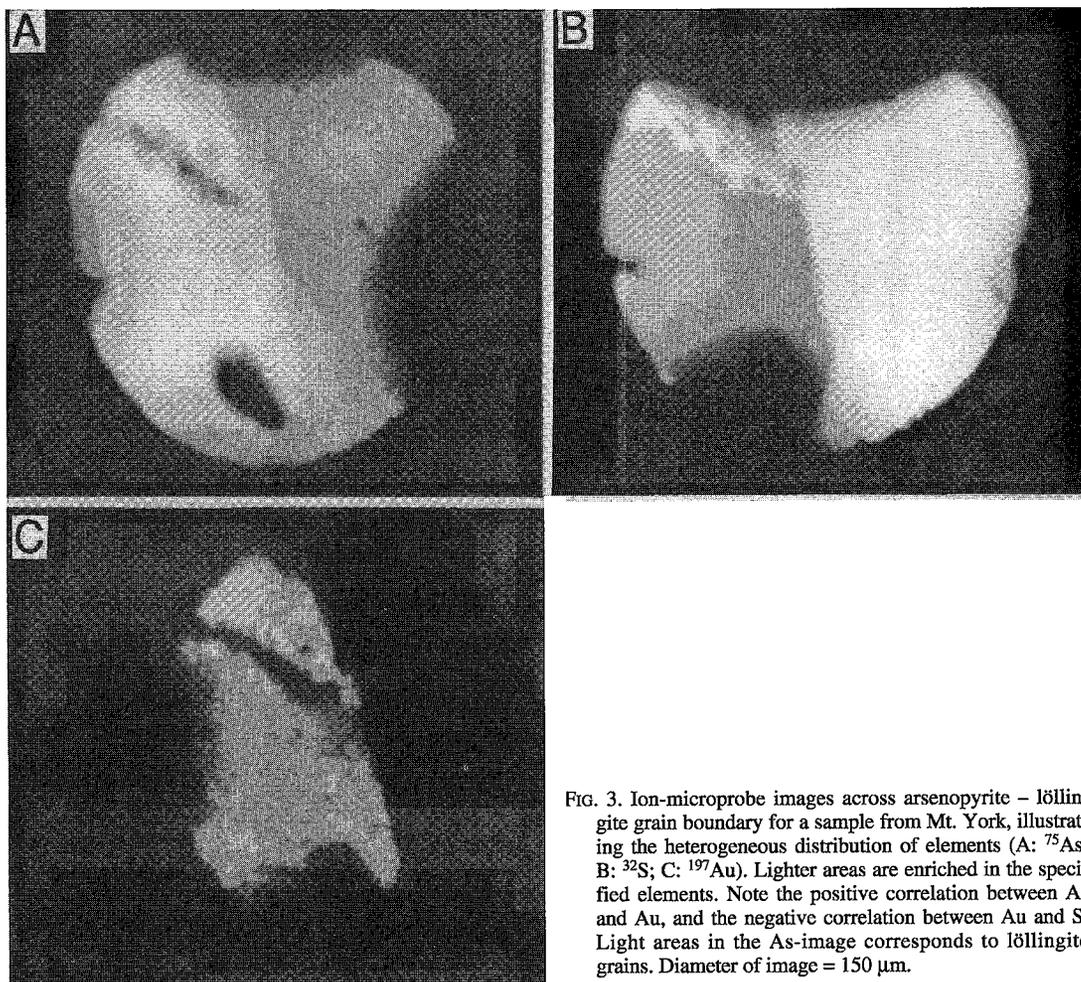
FIG. 3. Ion-microprobe images across arsenopyrite – löllingite grain boundary for a sample from Mt. York, illustrating the heterogeneous distribution of elements (A: ^{75}As; B: ^{32}S; C: ^{197}Au). Lighter areas are enriched in the specified elements. Note the positive correlation between As and Au, and the negative correlation between Au and S. Light areas in the As-image corresponds to löllingite grains. Diameter of image = 150 μm.

in addition, a voltage offset to eliminate the interfering molecular ions (Chryssoulis 1989). Minimum limits of detection were obtained using high mass-resolution; under optimum conditions, background levels were reduced to about 0.150 μg/g (150 ppb) for arsenopyrite and 0.050 μg/g (50 ppb) for löllingite. Digital imaging of Au, S, As and molecular ions in different minerals was carried out with beam currents of about 250 nA over areas 62.5 μm in diameter (in high mass-resolution) using a Resistive Anode Encoder (*cf.* Elphick *et al.* 1991). Line scans derived from these digital images are shown in Figure 5.

MINERALOGICAL DISTRIBUTION OF GOLD IN ORE AGGREGATES

Ore mineralogy

The ore mineralogy of both deposits is dominated by löllingite, arsenopyrite and pyrrhotite, with minor sphalerite and chalcopyrite. Coarse-grained Fe–As–S phases occur commonly as composite aggregates at Griffin's Find, whereas at Mt. York, both composite arsenopyrite – löllingite aggregates and discrete grains of arsenopyrite occur. Composite grains in both deposits generally have a core of löllingite mantled by arsenopyrite (*cf.* Ramdohr 1980, Fig. 504). The reverse zonation, with a core of arsenopyrite rimmed by löllingite, is never developed. Löllingite grains are everywhere separated from pyrrhotite by grains of arsenopyrite. Composite grains commonly have a single large core of löllingite rimmed by a thin band of unzoned arsenopyrite, although smaller cores of löllingite are present at Griffin's Find (Fig. 2). At Mt. York, several small, ovoid cores of löllingite are common within large grains of arsenopyrite (Fig. 2). Textures in both deposits suggest a progressive replacement of löllingite by arsenopyrite, leaving remnants of unre-
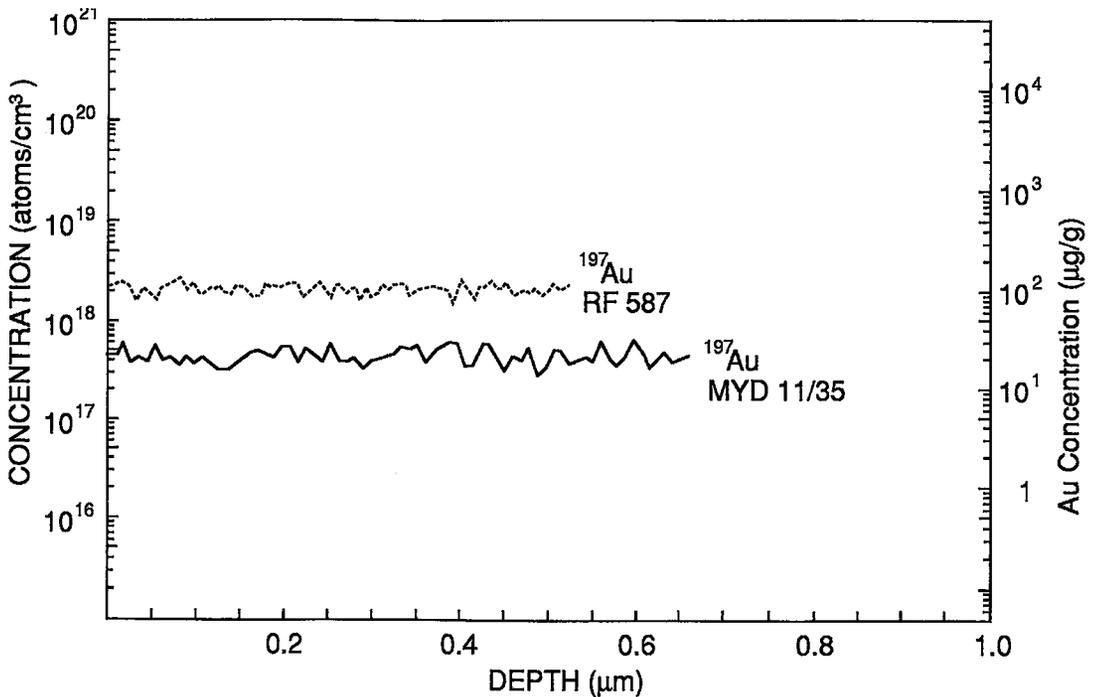
FIG. 4. Ion-microprobe depth profile of löllingite grains from Mt. York (solid line) and Griffin's Find (dotted line) for ^{197}Au. No inclusions of particulate gold can be identified in the profiles.

placed löllingite behind. At Griffin's Find, several adjacent grains of löllingite in different optical orientations (Fig. 2) are rimmed by a single arsenopyrite grain of constant optical orientation, indicating that several grains of löllingite were replaced by arsenopyrite. At Mt. York, at least two generations of arsenopyrite are present in some composite grains. Earlier arsenopyrite, which contains some inclusions of löllingite, is fractured and then recemented by a second generation of arsenopyrite (Fig. 2). Anhedral pyrrhotite is generally present as the dominant phase,

either as a rim or as inclusions within composite arsenopyrite – löllingite grains in both deposits. Composite arsenopyrite – löllingite grains are anhedral to subhedral, whereas the mantling euhedral arsenopyrite generally seems idioblastic within the pyrrhotite. The inner grain-boundary of the arsenopyrite against the löllingite is either straight or irregular and embayed (Fig. 2). In summary, all ore textures, observed optically or by SEM, suggest that a pre-

TABLE 1. STANDARDS USED FOR QUANTITATIVE SIMS ANALYSES

Standard	Peak Depth Å	Analytical Session	Matrix Species	RSF*
Asp-1	1960	Session I	S_2^-	1.97E+21
Asp-1	2070	Session I	S_2^-	2.04E+21
Asp-1	2223	Session II	FeAs$^-$	7.27E+19
Asp-1	2140	Session II	FeAs$^-$	7.40E+19
Asp-1	2080	Session III	FeAsS$_2^-$	4.39E+18
Asp-1	2200	Session III	FeAsS$_2^-$	4.49E+18
Lo-1	2200	Session II	FeAs$^-$	1.71E+20
Lo-1	2170	Session II	FeAs$^-$	1.59E+20
Lo-1	2180	Session II	FeAs$^-$	1.63E+20
Lo-1	2170	Session III	Fe$_2$As$^-$	2.01E+18
Lo-1	2180	Session III	Fe$_2$As$^-$	2.33E+18

Asp-1 = arsenopyrite; Lo-1 = löllingite; *RSF = Relative Sensitivity Facto measurements made under high mass resolution (M/AM = 4,000-4,800)

TABLE 2. RESULTS OF SIMS SPOT ANALYSES FOR Au IN ARSENOPYRITE AND LÖLLINGITE IN SAMPLES FROM MT. YORK AND GRIFFIN'S FIND

Mt. York			Griffin's Find		
Sample	Mineral	Au(μg/g)	Sample	Mineral	Au(μg/g)
11/35-1	apy	0.69	RF601A-1	apy	0.28
11/35-2	apy	0.16	RF601A-2	apy	0.66
11/35-3	apy	0.17	RF601A-3	lö	253*
11/35-4	apy	1.04*	RF601A-4	lö	275
11/35-5	lö	33.0*	RF601A-5	lö	199
11/35-6	lö	29.9	RF601A-6	lö	192
11/35-7	lö	20.1	RF601A-7	lö	134
11/35-8	lö	19.8	RF587A-1	apy	3.36
11/35-9	lö	28.2	RF587A-2	apy	0.43
			RF587A-3	lö	70.1
			RF587A-4	lö	182

Apy = arsenopyrite, lö = löllingite. *A calibration factor (as opposed to an RSF) was applied in cases where the Au counts were ratioed against Au counts from a different mineral when standards where not available. For example, Au counts from löllingite were compared with Au counts from the arsenopyrite standard.
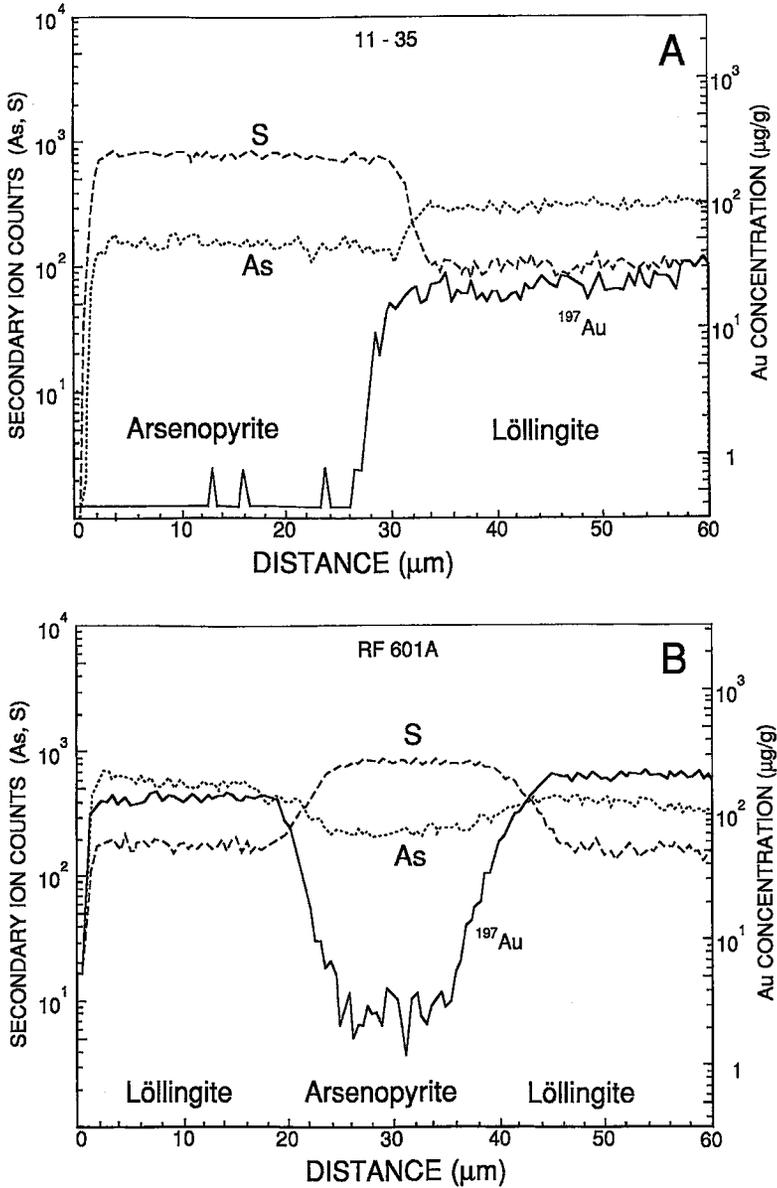
FIG. 5. Ion-microprobe scan across arsenopyrite – löllingite grain boundaries for samples from Mt. York (A) and Griffin's Find (B) for ^{75}As, ^{32}S and ^{197}Au. The data depicted were obtained by constructing linescans from the stored digital images. The distribution of arsenopyrite and löllingite is indicated. Note that gold is almost entirely restricted to the löllingite grain.

existing core of sulfur-poor löllingite was subsequently replaced by the more sulfur-rich arsenopyrite.

At Mt. York, metasomatic pyrrhotite and arsenopyrite occur as inclusions in garnet, grown at the peak of metamorphism, and pyrrhotite occurs as inclusions in deformed metamorphic magnetite in the outer, distal envelope of alteration. Pyrrhotite also is intergrown with amphibole in the inner, proximal zone of alteration. Hence the sulfide–arsenide assemblage is in textural equilibrium with metamorphic and metasomatic silicate and oxide minerals, which formed during or close to the peak of amphibolite-facies metamorphism

in the BIF at Mt. York (Neumayr *et al.* 1994).

Fare (1989) interpreted the ore assemblage at Griffin's Find as being synchronous with granulite-facies regional metamorphism, since: i) the grain size of the sulfides is similar to that of the silicate minerals, and ii) the sulfides are texturally part of the high-grade granulite-facies fabric (*e.g.*, metasomatic clinopyroxene encloses, and is enclosed by, sulfide minerals). A premetamorphic origin for the sulfides can be excluded, because mineralized quartz veins contain inclusions of garnet from the garnet granulite wallrock, and the quartz veins are only weakly deformed and contain primary fluid inclusions. A postmetamorphic, retrograde introduction of sulfides at Griffin's Find also can be excluded, since there is no evidence for pervasive retrogression of the wallrocks immediately adjacent to the ore zone, nor of retrograde alteration of the silicate minerals adjacent to the sulfides in the ore zone. The high thermodynamic variance of the assemblages attributed to metasomatic alteration and compositional zoning in individual phases (*e.g.*, clinopyroxene) argue strongly for peak-metamorphic formation of the silicates intermixed with the ore sulfides and arsenides (*e.g.*, Barnicoat *et al.* 1991).

Distribution of gold

Most of the gold mineralization, at both Mt. York and Griffin's Find, is closely associated with composite arsenopyrite –löllingite grains (*e.g.*, Croxford 1987), and microscopically visible gold is commonly concentrated at the arsenopyrite – löllingite grain boundary (Fig. 2; Nickel 1981, Neumayr *et al.* 1994). It rarely occurs within arsenopyrite, or at the arsenopyrite – pyrrhotite grain boundary, and is absent in monomineralic aggregates of arsenopyrite at Mt. York. Visible gold is normally ovoid, 5–25 μm in length, and occurs as single grains or in clusters of as many as 20 inclusions within a composite arsenopyrite – löllingite grain (Fig. 2). Compositions of individual inclusions of gold from Mt. York are summarized in Table 3. They generally contain up to 9.2 wt.% Ag, and the fineness [1000*(Au/(Au+Ag)] ranges from 908 to 916. Discrete grains of native gold at Griffin's Find are only rarely observed; the grains are small, but

can be up to 20 μm in length, with a fineness of approximately 750 (Fare & McNaughton 1990).

Samples from both deposits have been investigated by SIMS to test for the presence and distribution of "invisible" gold, *i.e.*, gold that is present either as: i) submicroscopic, submicrometric inclusions within a host mineral (colloidal gold), or as ii) solid solution or chemically bound gold (first described in pyrite: Bürg 1930). Samples of both arsenopyrite – löllingite grains containing inclusions of visible (optically or SEM) gold, and those free of visible inclusions of gold, were investigated by SIMS, using four different techniques: i) isotope images for ^{75}As, ^{32}S and ^{197}Au to examine the spatial distribution of gold in arsenopyrite and löllingite, ii) quantitative spot-analysis for gold in the different host-minerals, iii) line-scans for the isotopes ^{75}As, ^{32}S and ^{197}Au across grain boundaries between arsenopyrite and löllingite, and iv) quantitative depth-profiles for ^{197}Au in single spots, to test whether gold is present as subsurface inclusions in arsenopyrite and löllingite.

Figure 3 shows SIMS images that depict ^{75}As, ^{32}S and ^{197}Au abundances for the same field of view. Clearly, gold is associated with the phase with high As and lower S content (*i.e.*, löllingite, FeAs$_2$), whereas S-rich, relatively As-poor grains (*i.e.*, arsenopyrite, FeAsS) show no detectable gold with this method. The boundary between arsenopyrite and löllingite is sharp, and the "invisible" gold terminates at the grain boundary. SIMS spot analyses for gold in selected grains of löllingite and arsenopyrite (Table 2) show that löllingite at Mt. York contains 20–33 μg/g Au, whereas arsenopyrite in the same sample contains 0.16–1.04 μg/g Au. Two samples from Griffin's Find give similar results, but gold in löllingite is relatively enriched at 70–275 μg/g, and gold in arsenopyrite can be slightly higher than that at Mt. York at 0.28 to 3.36 μg/g.

An attempt was made to verify the presence of subtle indications of a concentration gradient of gold in arsenopyrite near löllingite – arsenopyrite grain boundaries. Within a distance of about 100 μm from the löllingite contact, analysis 11/35–1 with 0.69 μg/g Au is the nearest to the löllingite contact, whereas 11/35–2 is further away and 11/35–3 is furthest, both with about 0.16 μg/g Au. Likewise, analysis RF601A–2 (0.66 μg/g) is located nearer to the löllingite contact than is RF601A–1 (0.28 μg/g), which is about 75 μm further away, suggesting a slight concentration of gold in arsenopyrite near the löllingite contact in both Mt. York and Griffin's Find samples.

Figure 4 depicts two representative depth-profiles for samples of gold-bearing löllingite from Mt. York and Griffin's Find, designed to detect the presence of any submicrometric inclusions of gold. However, no such inclusions were detected in any samples. The exact size of detectable inclusions for the SIMS is dependent on conditions of analysis, but generally is

TABLE 3. RESULTS OF ENERGY–DISPERSION SEM ANALYSES OF GOLD INCLUSIONS IN COMPOSITE ARSENOPYRITE–LÖLLINGITE GRAINS OF THE MAIN HILL PROSPECT, MT. YORK

Sample	Au1	Au2	Au3	Au4	Au5
Au	90.88	90.78	90.90	89.79	90.46
Ag	9.18	8.94	8.30	8.84	9.05
Fe*	0.85	0.90	1.57	0.83	1.18
Total	100.90	100.60	100.80	99.45	100.70
Fineness	908	910	916	910	909

Concentrations quoted in wt.%. Fineness = 1000[Au/(Au + Ag)].
* Probably due to contamination by host phase.

less than 0.1 to 0.2 μm. The scatter in the lines in Figure 4 represents uncertainties in the analysis and does not indicate the presence of inclusions of gold, although the possibility of particulate gold that is finer-grained than the sampling volume of the SIMS (*i.e.*, colloidal gold) cannot be ruled out.

Line-scans across arsenopyrite – löllingite grain boundaries (Figs. 5A, B) confirm results obtained by SIMS imaging and spot analyses. A sharp but slightly sloping boundary exists between löllingite and arsenopyrite grains, and gold content is very low in most grains of arsenopyrite. The slight slope may relate to a slight increase in Au concentration in arsenopyrite nearest the boundary of a löllingite grain, as indicated by the spot analyses described above, but over a smaller distance for a narrower grain of arsenopyrite. Some spikes in the [197]Au line spectrum may represent variations in the distribution of gold in the arsenopyrite from Mt. York. The line-scan plot for the Griffin's Find sample shows similar relationships.

INTERPRETATION OF
SULFARSENIDE MINERAL TEXTURES

Textures in the sulfarsenides clearly indicate that arsenopyrite replaced löllingite, because: i) arsenopyrite everywhere rims single or multiple cores of löllingite, and the reverse is not observed, ii) arsenopyrite in one optical orientation rims aggregates of several grains of löllingite in different orientations, iii) the embayed grain boundaries between arsenopyrite and löllingite, and the presence of multiple löllingite cores in the Mt. York assemblage, suggest progressive replacement, and iv) at least two generations of arsenopyrite are present at Mt. York, with the latter cementing brecciated earlier arsenopyrite, which itself contains cores of löllingite. The occurrence of these textures in other lode-gold deposits worldwide (*e.g.*, Lhotka & Nesbitt 1989, McCuaig *et al.* 1994) implies that similar and recurrent processes were active during ore formation. However, few detailed studies on high-
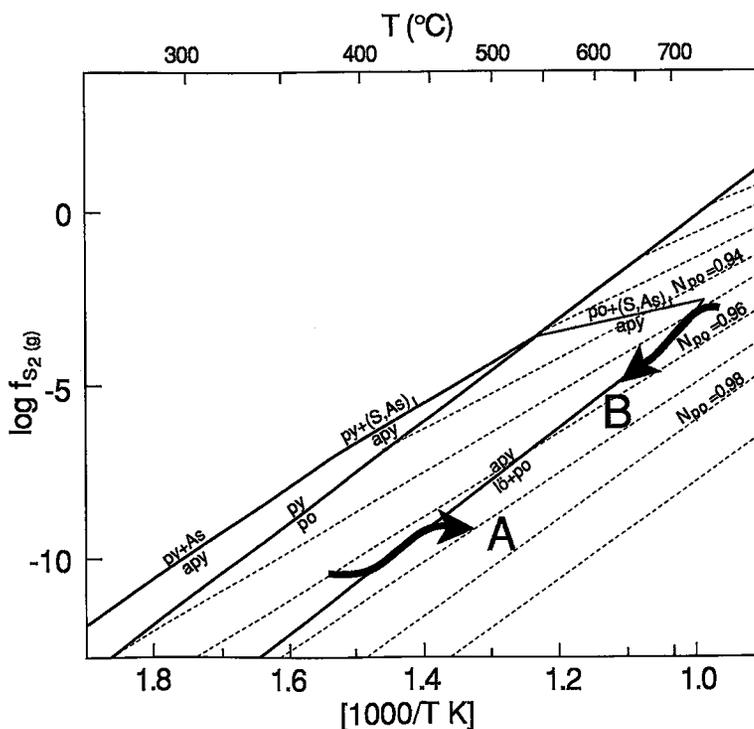

FIG. 6. Phase relations in the Fe–As–S system as a function of temperature and $f(S_2)_g$ at 3 kbar pressure. Schematic paths for prograde (A) and retrograde (B) metamorphic (solid-state) reactions between arsenopyrite and löllingite are indicated by heavy arrows. Compositional contours for pyrrhotite (dashed lines) were modified from Toulmin & Barton (1964). As shown, pyrrhotite solid-solutions provide the major reservoir or sink of sulfur in such solid-state reactions. Thermodynamic data from SUPCRT '92 (Johnston *et al.* 1992), and modified from Barton & Skinner (1979), Sharp *et al.* (1985) and Clark (1966). Symbols: As arsenic, S sulfur, py pyrite, apy arsenopyrite, po pyrrhotite, lö löllingite, N_{po} = [FeS/(FeS+S_2)].

temperature Archean lode-gold deposits exist, and thus few investigators have attempted to explain these paragenetic relationships.

For Griffin's Find, Barnicoat *et al.* (1991) argued against simple prograde metamorphism of lower-metamorphic-grade mineralization, stating that prograde desulfidation reactions involving arsenopyrite, the dominant arsenide in greenschist- and lower-amphibolite-grade deposits, would lead to arsenopyrite cores rimmed and replaced by löllingite (Fig. 6), exactly the opposite of the observed textures. Such a model also is inconsistent with abundant textural and mineralogical evidence that most amphibolite- to granulite-facies lode-gold deposits formed at or near peak metamorphic temperatures (Ridley & Barnicoat 1990, Barnicoat *et al.* 1991, Groves *et al.* 1992).

Barnicoat *et al.* (1991) ruled out a retrograde reaction between löllingite and pyrrhotite to form arsenopyrite because silicate gangue assemblages associated with ore lack obvious evidence of retrogression. However, the extremely rapid rate of equilibration for even the most refractory sulfides and arsenides at amphibolite- and granulite-facies temperatures (*e.g.*, Barton 1970, Barton & Skinner 1979) suggests that slightly retrograde, solid–solid reactions between löllingite and pyrrhotite may occur independently of the silicate minerals, and thus at least partly account for the absence of mutual contacts between grains of these two phases. With decreasing temperature, löllingite would continually react with pyrrhotite to form arsenopyrite and a more sulfur-deficient pyrrhotite:

$$FeAs_2 + (1/x)FeS_{(1+x)} = 2FeAsS + ([1+x]/x)FeS \quad [1]$$
$$\text{lö} \qquad\quad \text{po} \qquad\qquad \text{apy} \qquad \text{po}$$
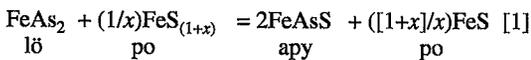
where x is less than or equal to 0.23. Reaction [1] would continue until löllingite cores were sufficiently shielded by arsenopyrite rims or temperatures dropped to the point where reaction was no longer kinetically favorable.

Although some of the arsenopyrite may therefore be retrograde in origin, much of the data presented above indicates a high-temperature hydrothermal origin for the majority of the arsenopyrite. Paragenetic and textural relationships between arsenide and sulfide phases, therefore, also reflect real changes in the environment of ore formation. Figure 7 summarizes the effects of ore-fluid chemistry on stability relationships of löllingite – arsenopyrite ($\pm$ pyrrhotite) at constant P–T conditions. As shown, ore-bearing fluids initially saturated in löllingite can move into the arsenopyrite field by increasing $a(H_2S)°$, decreasing $a(H_3AsO_3)°$ or by decreasing $a(H_2)(g)$ (oxidation) of the ore-bearing fluid. Such changes in composition of the ore fluid could reflect several different processes, including fluid–rock interaction, fluid mixing or changes in initial chemistry of the ore fluid with time. Furthermore, a moderate decrease in ore-fluid temperature also
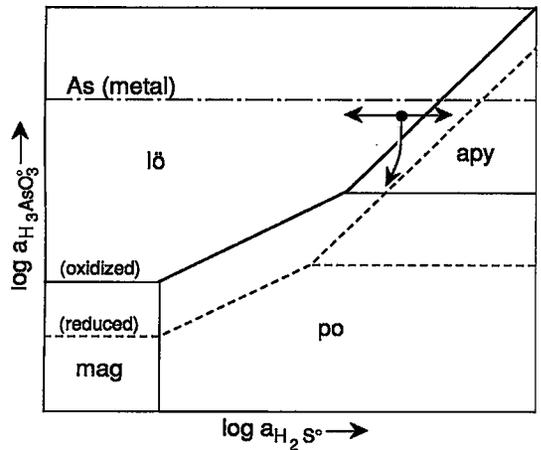

FIG. 7. Qualitative isothermal-isobaric phase relations for the Fe–As–S minerals as a function of the predominant species of arsenic and sulfur in solution at high P–T. Solid lines mark stability-field boundaries of minerals for moderately oxidizing [(low $a(H_2)_g$] conditions. Stability fields under reducing conditions are shown by light dashed lines, and illustrate the expansion of the löllingite field at high $a(H_2)_g$. The dotted-dashed line represents saturation limits for As metal in the ore fluid. Arrows show several potential evolutionary paths at constant $a(H_2)_g$ for ore fluids initially saturated in löllingite. As shown, observed paragenetic relationships necessitate a decrease in $a(H_3AsO_3)°$ in the ore fluid (either by precipitation of arsenic-bearing phases from solution or by mixing of the ore solution with an arsenic-poor hydrothermal fluid) or by an increase in $a(H_2S)°$. The latter, while potentially explaining the observed löllingite – arsenopyrite textures, would require fluid–rock interaction with unusually sulfur-rich host rocks or mixing with a more sulfur-rich fluid. Contraction of the stability field of löllingite at high oxidation-states suggests that oxidation of the ore fluid could also account for the change from löllingite- to arsenopyrite-saturated conditions under some circumstances. However, a drop in ore-fluid sulfur content resulting from sulfidation reactions in the wallrock is, by itself, unable to explain the observed paragenetic relationships (*cf.* Barnicoat *et al.* 1991). Symbols: mag magnetite; others as in Figure 6.

could result in a change from löllingite- to arsenopyrite-saturated conditions, provided redox conditions in the ore-bearing fluid were fluid-buffered (Fig. 8).

At present, it is difficult to assess which of the above processes, if any, is most important in controlling the löllingite – arsenopyrite textural relationships in amphibolite-facies lode-gold deposits. The relatively slow rates of cooling and reduced lateral temperature-gradients expected for the high-grade metamorphic conditions under which these deposits form argue against variations in temperature as the main mechanism. Barring isotopic or fluid-inclusion evidence for
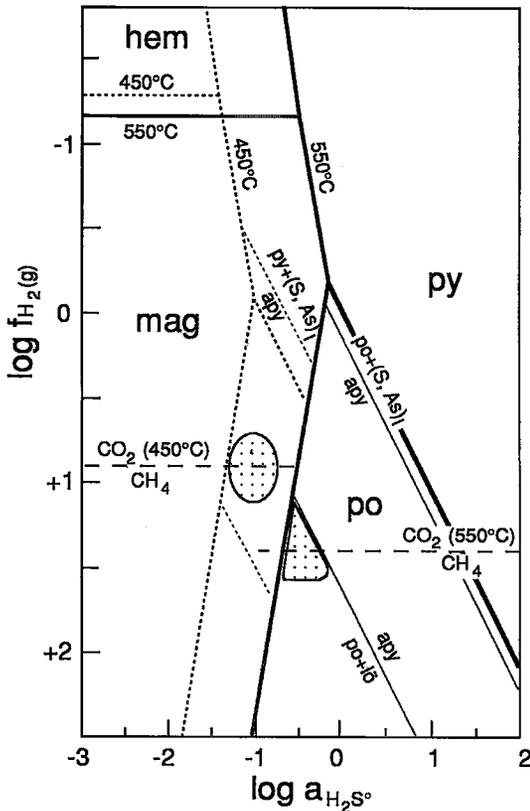
FIG. 8. Phase relations for Fe–As–S minerals as a function of $f(H_2)_g$ and $a(H_2S)°$ at 550°C (solid lines) and 450°C (dashed lines) and 3 kbar. Thick-dashed lines mark the locations of the CO_2/CH_4 redox buffer at these temperatures. Ore-fluid conditions for the Mt. York deposit (T=550°C) are shown by the shaded field, and broadly straddle the CO_2/CH_4 boundary. Cooling of the ore fluid under fluid-buffered redox conditions would maintain constant CO_2/CH_4 ratio in the ore fluid, thereby causing a change from löllingite- to arsenopyrite-saturated conditions with decreasing temperature (light-shaded field). Continued precipitation of pyrrhotite down temperature would result in a concomitant drop in the $a(H_2S)°$ of the ore fluid. Thermodynamic data and abbreviations as for Figure 6; in addition: hem hematite, mag magnetite.

fluid mixing in these types of deposit, interaction of the ore-bearing fluids with their surrounding host-rocks provides the most likely explanation. Gradients in both $a(H_2S)°$ and $a(H_3AsO_3)°$ would be expected during infiltration of sulfur- and arsenic-rich ore-bearing fluids into sulfur-poor, Fe-oxide- and Fe-silicate-bearing host rocks. Wallrock sulfidation and the resulting decrease in the H_2S content of the infiltrating ore-bearing fluid are, in fact, important mechanisms for gold deposition in greenschist-facies-hosted deposits (e.g., Neall & Phillips 1987). Depending on

the relative magnitudes of $H_2S°$ and $H_3AsO_3°$ depletion (Fig. 7), fluid–rock interaction of this type could explain both the observed paragenetic relationships and the lateral zonation in arsenopyrite:löllingite ratios observed for the Main Hill – Breccia Hill prospect.

<div align="center">INTERPRETATION OF PATTERNS
OF GOLD DISTRIBUTION</div>

Reflected-light microscopy, SEM and SIMS studies confirm that gold is closely associated with composite arsenopyrite – löllingite grains at Mt. York and Griffin's Find. Gold has been detected in both deposits in two different occurrences: i) as native gold, normally at arsenopyrite – löllingite grain boundaries and, much less commonly, within arsenopyrite or at the arsenopyrite–pyrrhotite contact, and, ii) as "invisible" gold in löllingite, within composite löllingite – arsenopyrite grains.

"Invisible" gold in löllingite could be present in two different forms: i) particulate (colloidal-size) gold as submicrometric inclusions, or ii) gold chemically bound in the structure of löllingite. The results of the SIMS depth profiling (Fig. 4) do not unequivocally define the state of the gold in löllingite from either Griffin's Find or Mt. York. There are also no other published data on the state of gold within löllingite. Discrete particles of native gold, 0.05–0.2 μm in diameter, enclosed in pyrite, cinnabar and, more rarely, in quartz have been reported by Bakken *et al.* (1989) from the Carlin sediment-hosted gold deposit. However, Mössbauer studies on arsenopyrite (Wagner *et al.* 1986) have confirmed that chemically bound gold also exists. Cathelineau *et al.* (1989) concluded, from similar studies on arsenopyrite, that gold is most likely present as a substituted element in the FeAsS structure, but the possible presence of submicrometric inclusions cannot be excluded. Cabri *et al.* (1989) examined arsenopyrite containing "invisible" gold with high-resolution transmission electron microscopy (HRTEM), but could not locate any particulate gold within the arsenopyrite; they concluded that, at least for the sections of arsenopyrite analyzed, no submicrometric inclusions are present.

In summary, it is likely that most of the "invisible" gold in arsenopyrite is chemically bound gold in solid solution, but this has only been proven in a few case-studies using Mössbauer techniques. By analogy, the "invisible" gold in löllingite from Griffin's Find and Mt. York also is very likely to be structurally bound. However, the presence of some colloidal "invisible" gold, less than 0.1–0.2 μm in diameter, cannot be completely excluded.

<div align="center">TIMING OF GOLD MINERALIZATION</div>

Gold is present in the samples as both visible and "invisible" gold, and the visible gold is concentrated at

Early   Late

Main Hill (Mt. York)	
Gold	. -————- .
Pyrrhotite	. -————- .
Löllingite	. -————- .
Arsenopyrite	. -————————- ..
Sphalerite	. -————- .
Chalcopyrite	. -————- .
Magnetite	. -————- .
Graphite	. -————- .
Amphibole	.- ————— ..
Carbonate	———— ..
Greenalite	. -——————— ..

Griffin's Find	
Gold	. -————- .
Löllingite	. -————- .
Pyrrhotite	. -————- .
Arsenopyrite	. -- ————————- .
Garnet	.- ————— .
Diopside	. -————- .
Graphite	. -- ———— .

Peak of metamorphism

FIG. 9. Summary of the paragenetic sequence for the assemblages of ore and alteration minerals at Main Hill (Mt. York) and at Griffin's Find.

arsenopyrite – löllingite grain boundaries. The evidence discussed above has established that löllingite was precipitated, together with pyrrhotite, broadly synchronously with the peak of metamorphism (Fig. 9). Since the majority of the "invisible" gold is contained within löllingite, coprecipitation of gold and löllingite is unequivocal, regardless of whether the gold is structurally bound or present as particulate colloidal-size gold. Arsenopyrite replaced löllingite either at conditions of peak metamorphism or in a slightly retrograde reaction. The selective occurrence of native gold at the arsenopyrite – löllingite interface, combined with the low concentrations of "invisible" gold in the arsenopyrite, suggest that at temperatures and pressures at or near those of the peak of metamorphism, löllingite was the preferred host for gold. During arsenopyrite formation, "invisible" gold was released from replaced löllingite to concentrate as native gold, preferentially at the arsenopyrite – löllingite interfaces.

There are some experimental data to support the notion that gold is not accepted in the arsenopyrite structure at the high-temperature conditions suggested here for ore deposition in the amphibolite- and granulite-facies gold deposits. Wagner et al. (1986) showed, using Mössbauer spectroscopy of a primary arsenopyrite – pyrite concentrate containing "invisi-

ble" gold and of the same concentrate after roasting, that structurally bound gold in the arsenopyrite can be released from the structure to form particulate gold at elevated temperatures. Cathelineau et al. (1989) reported on "Au-rich" arsenopyrite that formed at temperatures of $200 \pm 50°C$, and "Au-poor" arsenopyrite that formed at 300° to 500°C from the Hercynian belt in Europe. Heating experiments on synthetic arsenopyrite containing "invisible" gold, monitored in an analytical TEM, have shown that thermal treatment causes loss of As from the structure, producing a form of pyrrhotite and aggregation of the Au to form visible globules in a vacuum at 450°C, below the melting point of gold (Aylemore & Graham 1992). In the presence of oxygen, agglomeration of Au and loss of As can occur at even lower temperatures. These experiments indicate that Au is not stable in the arsenopyrite structure at elevated temperatures.

More experiments are needed to determine the temperatures of stability more accurately. However, the experiments can potentially explain the results from the Mt. York and Griffin's Find deposits, in which "invisible" gold is present in löllingite, but essentially absent in arsenopyrite. Gold was precipitated with löllingite broadly synchronously with the peak of metamorphism at elevated temperatures (>520°C: Mt. York, >700°C: Griffin's Find). The replacement of löllingite by arsenopyrite occurred at similar, or slightly lower temperatures, at which gold could not be incorporated into the arsenopyrite structure; the gold was consequently concentrated in particulate form at the replacement front. However, detailed experiments must be conducted to understand the mechanisms of substitution of gold in the löllingite and arsenopyrite structures at temperatures equivalent to the amphibolite- and lower granulite-facies metamorphism to verify this explanation.

CONCLUSIONS

This multidisciplinary study, utilizing a combination of conventional reflected-light microscopy, SEM, and quantitative SIMS analysis for trace-element analysis of sulfides, has helped to resolve the problem of the mineralogical distribution of gold and the timing of gold mineralization in two Archean lode-gold deposits from high-metamorphic-grade settings. The work has demonstrated that at Mt. York and Griffin's Find:
i) gold is closely associated with composite arsenopyrite – löllingite grains;
ii) gold has initially been precipitated together with löllingite, most probably in solid solution, as structurally bound gold in löllingite, or less likely as colloidal gold, at temperatures corresponding to amphibolite- and lower-granulite-facies metamorphism, respectively;
iii) gold has been liberated from the löllingite structure

and concentrated at arsenopyrite – löllingite grain boundaries during the replacement of löllingite by arsenopyrite under slightly retrograde conditions at similar, or less likely, increased activity of S_2;

iv) on the basis of natural and available experimental systems, it appears that the formation of native gold resulted from the inability of arsenopyrite to incorporate gold in its structure at high temperatures;

v) gold was introduced early into the system, mainly during precipitation of löllingite, in contrast to the late gold commonly documented in quartz–gold veins in settings at lower metamorphic grade.

It is important to note that the deposition of gold would have been considered retrograde (and therefore late) in the two deposits studied here if only the textural relations of the visible native gold had been considered. This inference stresses the need for careful determinations of the distribution of gold before paragenetic interpretations are made based solely on textural relationships involving native gold and other minerals.

REFERENCES

ANDREWS, A.J., HUGON, H., DUROCHER, M., CORFU, F. & LAVIGNE, M.J. (1986): The anatomy of a gold-bearing greenstone belt: Red Lake, northwestern Ontario, Canada. In Proc. Gold '86 – an International Symposium on the Geology of Gold Deposits (A. J. Macdonald ed.). Toronto (3-22).

AYLEMORE, M.G. & GRAHAM, J. (1992): Arsenopyrite as a host for refractory gold. In Proc. ACEM-12 & ANZSCB-11: The 1992 Joint Conf. on Electron Microscopy and Cell Biology: Electron microscopy in mining, exploration and metallurgy (B.J. Griffin, A.W.S. Johnson, J. Kuo & F.J. Lincoln, eds.). Perth (43).

BAKKEN, B.M., HOCHELLA, M.F., JR., MARSHALL, A.F. & TURNER, A.M. (1989): High-resolution microscopy of gold in unoxidized ore from the Carlin mine, Nevada. Econ. Geol. 84, 171-179.

BARNICOAT, A.C., FARE, R.J., GROVES, D.I. & McNAUGHTON, N.J. (1991): Synmetamorphic lode-gold deposits in high-grade Archaean settings. Geology 19, 921-924.

BARTON, P.B., JR. (1970): Sulfide petrology. Mineral. Soc. Am., Spec. Pap. 3, 187-198.

———— & SKINNER, B.J. (1979): Sulfide mineral stabilities. In Geochemistry of Hydrothermal Ore Deposits (H.L. Barnes, ed.). John Wiley & Sons, New York (278-403).

BOIRON, M.-C., CATHELINEAU, M., ESSARAJ, S., LESPINASSE, M. & SELLIER, E. (1991): Characterization of the relationships between deformation, fluid migration and Au deposition in quartz veins: methodology and modelling. In Proc. Gold '91 – The Economics, Geology, Geochemistry and Genesis of Gold Deposits (E.A. Ladeira, ed.). Balkema, Rotterdam (637-643).

BÜRG, G.H. (1930): Die Sichtbarmachung des feinverteilten Goldes in goldhöffigen Erzen und ihre wirtschaftliche Bedeutung. Metall. u. Erz 27, 333-338.

BURK, R., HODGSON, C.J. & QUARTERMAIN, R.A. (1986): The geological setting of the Teck–Corona Au–Mo–Ba deposit, Hemlo, Ontario, Canada. In Proc. Gold '86, an International Symposium on the Geology of Gold Deposits (A.J. Macdonald, ed.). Toronto (311-326).

CABRI, L.J. & CHRYSSOULIS, S.L. (1990): Advanced methods of trace-element microbeam analyses. In Advanced Microscopic Studies of Ore Minerals (J.L. Jambor & D.J. Vaughan, eds.). Mineral. Assoc. Can., Short-Course Handbook 17, 341-377.

————, ————, DE VILLIERS, J.P.R., LAFLAMME, J.H.G. & BUSECK, P.R. (1989): The nature of "invisible" gold in arsenopyrite. Can. Mineral. 27, 353-362.

CATHELINEAU, M., BOIRON, M.-C., HOLLIGER, P., MARION, P. & DENIS, M. (1989): Gold in arsenopyrites: crystal chemistry, location and state, physical and chemical conditions of deposition. In The Geology of Gold Deposits: the Perspective in 1988 (R.R. Keays, R. Ramsay & D.I. Groves, eds.). Econ. Geol., Monogr. 6, 328-341.

CHRYSSOULIS, S.L. (1989): Quantitative trace metal analysis of sulfide and sulfarsenide minerals by SIMS. In Secondary Ion Mass Spectroscopy, SIMS VII, Proc. (A. Benninghoven, C.A. Evans, K.D. McKeegan, H.A. Storms & H.W. Werner, eds.). John Wiley & Sons, New York (405-408).

————, CABRI, L.J. & LENNARD, W. (1989): Calibration of the ion microprobe for quantitative trace precious metal analyses of ore minerals. Econ. Geol. 84, 1684-1689.

————, ———— & SALTER, R.S. (1987): Direct determination of invisible gold in refractory sulphide ores. In Proc.

International Symposium on Gold Metallurgy (R.S. Salter, D.M. Wyslouzil & G.W. McDonald, eds.). *Proc. Metall. Soc., Can. Inst. Mining Metall.* **1**, 235-244.

CLARK, S.P., JR. (1966): High-pressure phase equilibria. *In* Handbook of Physical Constants (S.P. Clark, Jr., ed.). *Geol. Soc. Am., Mem.* **97**, 345-370.

COLVINE, A.C., FYON, J.A., HEATHER, K.B., MARMONT, S., SMITH, P.M. & TROOP, D.G. (1988): Archean lode gold deposits in Ontario. *Ont. Geol. Surv., Misc. Pap.* **139**.

COUTURE, J.F. & GUHA, J. (1990): The Eastman River deposit: a syntectonic shear zone hosted vein-type gold deposit in an amphibolite grade setting. *In* Proc. Nuna Research Conf., Greenstone Gold and Crustal Evolution (F. Robert, P.A. Sheahan & S.B. Green, eds.). *Geol. Assoc. Can. – Soc. Econ. Geol.*, 147 (abstr.).

CROXFORD, N.J.W. (1987): Mineralogical and metallurgical aspects of the Mount York gold deposit. *Mount Isa Mines Exploration internal report* **987-723**.

ELPHICK, S.C., GRAHAM, C.M., WALKER, F.D.L. & HOLNESS, M.B. (1991): The application of SIMS ion imaging techniques in the experimental study of fluid–mineral interactions. *Mineral. Mag.* **55**, 347-356

FARE, R.J. (1989): *Nature, Timing, and Genesis of a Granulite-Facies Gold Deposit at Griffin's Find, Western Gneiss Terrain, Western Australia*. Honours B.Sc. thesis, The University of Western Australia, Nedlands, Australia.

———— & MCNAUGHTON, N.J. (1990): Griffin's Find. *In* Gold Deposits of the Archaean Yilgarn Block, Western Australia: Nature, Genesis and Exploration Guides (S.E. Ho, D.I. Groves & J.M. Bennett, eds.). *Department of Geology (Key Centre) & University Extension, The University of Western Australia (Nedlands)* **20**, 182-184.

GROVES, D.I., BARLEY, M.E., BARNICOAT, A.C., CASSIDY, K.F., FARE, R.J., HAGEMANN, S.G., HO, S.E., HRONSKY, J.M.A., MIKUCKY, E.J., MÜLLER, A.G., MCNAUGHTON, N.I., PERRING, C.S., RIDLEY, J.R. & VEARNCOMBE, J.R. (1992): Sub-greenschist to granulite-hosted Archaean lode-gold deposits at the Yilgarn Craton: a deposition and continuum from deep-sourced hydrothermal fluids in crustal-scale, plumbing systems. *In* Proc. Third Int. Archaean Symp. (Perth) – The Archaean Terrains, Processes and Metallurgy (J.E. Glover & S.E. Ho, eds.). *Department of Geology (Key Centre) and University Extension, The University of Western Australia (Nedlands)* **22**, 325-337.

HAMILTON, J.V. & HODGSON, C.J. (1986): Mineralization and structure of the Kolar gold field, India. *In* Proc. Gold '86 – an International Symposium on the Geology of Gold Deposits (A.J. Macdonald, ed.). Toronto (270-283).

HOLDAWAY, M.J. (1971): Stability of andalusite and the aluminum silicate phase diagram. *Am. J. Sci.* **271**, 97-131.

JOHNSTON, J.W., OELKERS, E.H. & HELGESON, H.C. (1992): SUPCRT '92: A software package for calculating the structural molal thermodynamic properties of minerals, gases, aqueous species and reactions from 1 to 5000 bars and 0°C to 1000°C. *Computers and Geosci.* **17**, 899-947.

KOJONEN, K., JOHANSON, B. & SIPILÄ, E. (1991): The Kiimala deposit in Haapavesi, western Finland. *In* Geological Survey of Finland, Current Research 1989–1990 (S. Autio, ed.). *Geol. Surv. Finland, Spec. Pap.* **12**, 75-79.

KONTONIEMI, O., JOHANSON, B., KOJONEN, K. & PAKKANEN, L. (1991): Ore mineralogy of the Osikonmäki gold deposit, Rantasalmi, southeastern Finland. *In* Geological Survey of Finland, Current Research 1989–1990 (S. Autio, ed.). *Geol. Surv. Finland, Spec. Pap.* **12**, 81-89.

KUHN, R.J., KENNEDY, P., COOPER, P., BROWN, P., MACKIE, R., KUSINS, R. & FRIESEN, R. (1986): Geology and mineralization associated with the Golden Giant Deposit, Hemlo, Ontario, Canada. *In* Proc. Gold '86 – an International Symposium on the Geology of Gold Deposits (A.J. Macdonald, ed.). Toronto (327-339).

LHOTKA, P.G. & NESBITT, B.E. (1989): Geology of unmineralized and gold-bearing iron formation, Contwoyto Lake – Point Lake region, Northwest Territories, Canada. *Can. J. Earth Sci.* **26**, 46-64.

MARMONT, S. (1986): The geological setting of the Detour Lake gold mine, Ontario Canada. *In* Proc. Gold '86 – an International Symposium on the Geology of Gold Deposits (A.J. Macdonald, ed.). Toronto (81-96).

MCCUAIG, T.C., KERRICH, R., GROVES, D.I. & ARCHER, N. (1994): The nature and dimensions of regional and local gold-related hydrothermal alteration in tholeiitic metabasalts in the Norseman goldfields: the missing link in a crustal continuum of gold deposits? *Mineral. Deposita* (in press).

MCNAUGHTON, N.J., COMPSTON, W. & BARLEY, M.E. (1993): Constraints on the age of the Warrawoona Group, eastern Pilbara Block, Western Australia. *Precambrian Res.* **60**, 69-98.

NEALL, F.B. & PHILLIPS, G.N. (1987): Fluid – wall-rock interaction in an Archaean hydrothermal gold deposit: a thermodynamic model for the Hunt mine, Kambalda. *Econ. Geol.* **82**, 1679-1694.

NEUMAYR, P., GROVES, D.I., RIDLEY, J.R. & KONING, C.D. (1994): Syn-amphibolite-facies Archaean lode-gold mineralization in the Mt. York District, Pilbara Block, Western Australia. *Mineral. Deposita* (in press).

NICKEL, E.H. (1981): The mineralogy and geochemistry of the gold deposit at Griffin's Find, Western Australia. Otter Exploration N.L. (unpubl. internal rep.).

PAN, YUANMING & FLEET, M.E. (1992): Calc-silicate alteration in the Hemlo gold deposit, Ontario: mineral assemblages, P–T–X constraints, and significance. *Econ. Geol.* **87**, 1104-1120.

PHILLIPS, G.N. (1990): Wallrock alteration around Big Bell: a pre-peak metamorphic gold deposit. *In* Gold Deposits of

the Archaean Yilgarn Block, Western Australia: Nature, Genesis and Exploration Guides (S.E. Ho, D.I. Groves & J.M. Bennet, eds.). *Department of Geology (Key Centre) & University Extension, The University of Western Australia (Nedlands)* **20**, 87-89.

———— & DE NOOY, D. (1988): High-grade metamorphic processes which influence Archaean gold deposits, with particular reference to Big Bell, Australia. *J. Metamorphic Geol.* **6**, 95-114.

RAMDOHR, P. (1980): *The Ore Minerals and their Intergrowths* (second edition). Pergamon Press, Oxford, U.K.

REED, S.J.B. (1989): Ion microprobe analysis – a review of geological applications. *Mineral. Mag.* **53**, 3-24.

RIDLEY, J.R. & BARNICOAT, A.C. (1990): Wallrock alteration in amphibolite-facies gold deposits. *In* Gold Deposits of the Archaean Yilgarn Block, Western Australia: Nature, Genesis and Exploration Guides (S.E. Ho, D.I. Groves & J.M. Bennet, eds.). *Department of Geology (Key Centre) & University Extension, The University of Western Australia (Nedlands)* **20**, 79-86.

ROBERT, F. & KELLY, W.C. (1987): Ore-forming fluids in Archean gold-bearing quartz veins at the Sigma mine, Abitibi greenstone belt, Quebec, Canada. *Econ. Geol.* **82**, 1464-1482.

SHARP, Z.D., ESSENE, E.J. & KELLY, W.C. (1985): A re-examination of the arsenopyrite geothermometer: pressure considerations and applications to natural assemblages. *Can. Mineral.* **23**, 517-534.

TABEART, C.F. (1987): Controls to deposition of gold, copper and bismuth at Renco mine, Zimbabwe. *In* African Mining, *Inst. Mining Metall., London* (347-363).

———— (1988): Microstructural and strain related controls to gold precipitation in Archaean shear zones – Renco gold mine in the Limpopo Belt, Zimbabwe. *In* Proc. Bicentennial Gold 88 – Extended Abstr. 2 (A.D.T. Goode, E.L. Smyth, W.D. Birch & L.I. Bosma, comp.).

Geol. Soc. Aust., Abstr. **23**, 122-124.

THORPE, R.I., HICKMAN, A.H., DAVIS, D.W., MORTENSON, J.K. & TRENDALL, A.F. (1990): Application of recent zircon U–Pb geochronology to the Marble Bar region, Pilbara Craton, to modelling Archaean lead evolution. *In* Third Int. Archaean Symposium – Extended Abstr. Vol. (J.E. Glover & S.E. Ho, comp.). *Geoconferences* (Perth, Western Australia), 11-13.

TOULMIN, P., III & BARTON, P.B., JR. (1964): A thermodynamic study of pyrite and pyrrhotite. *Geochim. Cosmochim. Acta* **28**, 641-671.

WAGNER, F.E., MARION, P.H. & REGNARD, J.-R. (1986): Mössbauer study of the chemical state of gold in gold ores. *In* Gold 100 – Proc. Int. Conf. on Gold, Vol. **2**: Extractive Metallurgy of Gold. *S. Afr. Inst. Mining Metall.* (435-443).

WHITE, W.H. (1943): The mechanism and environment of gold deposition in veins. *Econ. Geol.* **38**, 512-532.

WILDE, S.A. & PIDGEON, R.T. (1987): U–Pb geochronology, geothermometry and petrology of the main areas of gold mineralization in the Wheat Belt region of Western Australia. *Western Australian Mining and Petroleum Research Institute, Rep.* **30**.

WILSON, G.C., KILIUS, L.R. & RUCKLIDGE, J.C. (1991): *In situ* analysis of precious metals in polished mineral samples and sulphide "standards" by Accelerator Mass Spectrometry at concentrations of parts-per-billion. *Geochim. Cosmochim. Acta* **55**, 2241-2251.

WOOD, P.C., BURROWS, D.R., THOMAS, A.V. & SPOONER, E.T.C. (1986): The Hollinger – McIntyre Au–quartz vein system, Timmins, Ontario, Canada; geologic characteristics, fluid properties, and light stable isotope geochemistry. *In* Proc. Gold '86 – an International Symposium on the Geology of Gold Deposits (A. J. Macdonald, ed.). Toronto (56-80).